The Journal of Chemical Physics

RESEARCH ARTICLE | JULY 10 2023

Equilibrium molecular dynamics evaluation of the solid–liquid friction coefficient: Role of timescales

Haruki Oga ; Takeshi Omori ; Laurent Joly ; Yasutaka Yamaguchi

J. Chem. Phys. 159, 024701 (2023)
https://doi.org/10.1063/5.0155628

The Journal of Chemical Physics ARTICLE pubs.aip.org/aip/jcp

Equilibrium molecular dynamics evaluation of the solid–liquid friction coefficient: Role of timescales

Cite as: J. Chem. Phys. 159, 024701 (2023); doi: 10.1063/5.0155628
Submitted: 21 April 2023 • Accepted: 16 June 2023 •
Published Online: 10 July 2023

Haruki Oga,[1,a)] Takeshi Omori,[2,b)] Laurent Joly,[3,c)] and Yasutaka Yamaguchi[1,4,d)]

AFFILIATIONS

[1] Department of Mechanical Engineering, Osaka University, 2-1 Yamadaoka, Suita 565-0871, Japan
[2] Department of Mechanical Engineering, Osaka Metropolitan University, 3-3-138 Sugimoto, Sumiyoshi, Osaka 558-8585, Japan
[3] Univ Lyon, Univ Claude Bernard Lyon 1, CNRS, Institut Lumière Matière, F-69622 Villeurbanne, France
[4] Water Frontier Research Center (WaTUS), Research Institute for Science and Technology, Tokyo University of Science, 1-3 Kagurazaka, Shinjuku-ku, Tokyo 162-8601, Japan

[a)] **Electronic mail:** haruki@nnfm.mech.eng.osaka-u.ac.jp
[b)] **Electronic mail:** t.omori@omu.ac.jp
[c)] **Electronic mail:** laurent.joly@univ-lyon1.fr
[d)] **Author to whom correspondence should be addressed:** yamaguchi@mech.eng.osaka-u.ac.jp

ABSTRACT

Solid–liquid friction plays a key role in nanofluidic systems. Following the pioneering work of Bocquet and Barrat, who proposed to extract the friction coefficient (FC) from the plateau of the Green–Kubo (GK) integral of the solid–liquid shear force autocorrelation, the so-called plateau problem has been identified when applying the method to finite-sized molecular dynamics simulations, e.g., with a liquid confined between parallel solid walls. A variety of approaches have been developed to overcome this problem. Here, we propose another method that is easy to implement, makes no assumptions about the time dependence of the friction kernel, does not require the hydrodynamic system width as an input, and is applicable to a wide range of interfaces. In this method, the FC is evaluated by fitting the GK integral for the timescale range where it slowly decays with time. The fitting function was derived based on an analytical solution of the hydrodynamics equations [Oga *et al.*, Phys. Rev. Res. **3**, L032019 (2021)], assuming that the timescales related to the friction kernel and the bulk viscous dissipation can be separated. By comparing the results with those of other GK-based methods and non-equilibrium molecular dynamics, we show that the FC is extracted with excellent accuracy by the present method, even in wettability regimes where other GK-based methods suffer from the plateau problem. Finally, the method is also applicable to grooved solid walls, where the GK integral displays complex behavior at short times.

I. INTRODUCTION

Nanofluidics describes the motion of fluids confined at the nanoscale and plays an important role in various fields such as nanotechnology, biology, and energy conversion.[1–6] Solid–liquid (S–L) slip particularly affects fluid transport, and Navier proposed the following boundary condition (BC) as the slip model:[7]

$$\tau_\mathrm{w} = \lambda_0 u_\mathrm{slip}, \tag{1}$$

where τ_w is the S–L friction force per area, λ_0 is the S–L friction coefficient (FC), and u_slip is the slip velocity. Equation (1) is called the Navier BC. If Newton's law of viscosity is applied at the S–L interface, the shear force per area, i.e., shear stress, is given by

$$\tau_\mathrm{w} = \eta \left.\frac{\partial u}{\partial z}\right|_\mathrm{interface}, \tag{2}$$

where η and u are the liquid viscosity and the velocity parallel to the S–L interface as a function of the normal position z. Hence, the Navier BC in Eq. (1) can be written in another form as

$$\frac{u_\mathrm{slip}}{b} = \left.\frac{\partial u}{\partial z}\right|_\mathrm{interface}, \tag{3}$$

where b is called the slip length and is defined by

$$b = \frac{\eta}{\lambda_0}. \tag{4}$$

The slip length depends on the S–L combination; e.g., for water on a graphene or carbon nanotube surface, b was theoretically and experimentally estimated to be about several tens of nanometers.[8–10]

Molecular dynamics (MD) is a powerful tool to evaluate the FC, or slip length, and to explore the mechanisms underlying S–L friction.[8,11–22] The FC can be directly calculated by using non-equilibrium MD (NEMD) simulations of Poiseuille or Couette flows; however, this requires a high shear rate, typically above 10^9 s^{-1}, to reduce the statistical error due to thermal fluctuation. In such a range, the FC λ_0 can depend on the shear rate, i.e., the shear force τ_w is not proportional to the slip velocity u_slip as in Eq. (1).[14,23,24] In addition, the S–L interface position must be defined to strictly determine the slip velocity u_slip or the slip length b, which is not trivial.[25]

On the other hand, several methods for calculating the FC from equilibrium MD (EMD) with a zero shear rate have been proposed.[24,26–36] In their pioneering work, Bocquet and Barrat (BB)[26,29] introduced a Green–Kubo (GK) integral defined by

$$\Lambda(t) \equiv \frac{1}{Sk_\mathrm{B}T}\int_0^t \langle F_\mathrm{w}(t)F_\mathrm{w}(0)\rangle \mathrm{d}t, \tag{5}$$

where S, k_B, T, and $\langle F_\mathrm{w}(t)F_\mathrm{w}(0)\rangle$ denote the surface area, Boltzmann constant, absolute temperature, and equilibrium autocorrelation function of the instantaneous shear force F_w on the solid as a function of time t, respectively, for the calculation of the FC. In bulk systems, GK integrals are a standard tool to calculate transport properties; e.g., the viscosity of a fluid can be obtained from the autocorrelation of the off-diagonal stress component.[37] However, in contrast to bulk GK integrals, which show a simple behavior of monotonically increasing with time t and converging to a certain value for $t \to \infty$, $\Lambda(t)$ typically increases for a short time and decreases after taking a maximum, which we will call the intermediate plateau value, and usually converges to a non-zero final plateau value for $t \to \infty$. This behavior is often referred to as the plateau problem.[32,38,39] When the friction coefficient is small, i.e., the slip length is large, the intermediate plateau region of the GK integral $\Lambda(t)$ is clearly observed, and in such cases, it indeed gives a good estimate of the corresponding NEMD result.[32] However, for larger FC, $\Lambda(t)$ decays faster with time after taking a maximum; thus, the intermediate plateau region is not apparent, and the corresponding value of $\Lambda(t)$ is not well-defined.[32,38,39] Even in such a case, the FC is often estimated from the maximum value of the GK integral as[32,34,40]

$$\lambda_0 \approx \max[\Lambda(t)], \tag{6}$$

although it does not necessarily give a proper estimate.[32]

Recently, the authors derived an analytical expression of the GK integral $\Lambda(t)$ by explicitly modeling the liquid motion described by the Stokes equation. The expression of $\Lambda(t)$ includes a non-Markovian effect quantified by the friction kernel $\lambda(t)$,[41,42] with which the friction force per area $\tau_\mathrm{w}(t)$ at time t is expressed by

$$\tau_\mathrm{w}(t) = \int_{-\infty}^t \lambda(t-s)u_\mathrm{slip}(s)\mathrm{d}s, \tag{7}$$

including the hysteresis dependence of the slip velocity. For a steady flow with a constant slip velocity u_slip, the friction coefficient λ_0 in the Navier BC is related to this friction kernel $\lambda(t)$ by

$$\lambda_0 = \int_0^\infty \lambda(t)\mathrm{d}t. \tag{8}$$

For simple liquids at room temperature, the friction kernel $\lambda(t)$ typically decays within a short timescale, which we denote by t_fk, around several picoseconds. Considering this feature, the friction kernel is often modeled by the following Maxwell-type expression:[33,42,43]

$$\lambda(t) = \frac{\lambda_0}{t_\mathrm{fk}}e^{-\frac{t}{t_\mathrm{fk}}}. \tag{9}$$

Note that taking the limit of $t_\mathrm{fk} \to 0$ corresponds to a Markovian FC without a hysteresis effect. It has been shown that the Maxwell model in Eq. (9) approximates well the friction for various kinds of liquids, e.g., Lennard–Jones (LJ) liquids or water, on various solid surfaces,[33,42,43] and that $\Lambda(t)$ typically increases from zero and takes the maximum around t_fk, whereas for specific cases such as supercooled water, the simple Maxwell-type kernel is not sufficient to express $\lambda(t)$.[43] Related to this point, Hansen *et al.*[28,33] proposed to calculate the friction kernel $\lambda(t)$ by measuring the fluctuations of the S–L friction force and the slip velocity. Specifically, the authors used the cross-correlation of the force and velocity of a liquid slab adjacent to the solid surface as an alternative method to using the GK integral and avoided the plateau problem. In addition, Nakano and Sasa[34] derived an analytical expression of the GK integral $\Lambda(t)$ based on linearized fluctuating hydrodynamics (LFH) by assuming timescale separation, and they proposed a measurement method of λ_0 by fitting the GK integral with this analytical expression.

Overall, the understanding of the solid–liquid FC and the related GK integral has progressed significantly during the last few years. In this context of active development of methods to calculate the FC from EMD, we propose here a new approach based on time separation in the GK integral $\Lambda(t)$. We compare this approach to NEMD and existing GK-based methods, and we highlight the advantages of the new method.

II. THEORY

Let us consider a system where a liquid is confined between two fixed planar solid walls. The authors derived a theoretical expression of the equilibrium autocorrelation function of the S–L friction force $C_{F_\mathrm{w}}(t) \equiv \langle F_\mathrm{w}(t)F_\mathrm{w}(0)\rangle$ for that system—which is the differential of the GK integral $\Lambda(t)$ as shown in Eq. (5)—by coupling the Stokes equation for the liquid motion and a Langevin equation for the motion of one of the walls in the direction parallel to the interface, using the Fourier–Laplace (FL) transform as[43]

$$\frac{\tilde{C}_{F_\mathrm{w}}(\omega)}{Sk_\mathrm{B}T} = \frac{\tilde{\lambda}\eta\zeta[\eta\zeta\sinh(\zeta h) + \tilde{\lambda}\cosh(\zeta h)]}{(\tilde{\lambda}^2 + \eta^2\zeta^2)\sinh(\zeta h) + 2\tilde{\lambda}\eta\zeta\cosh(\zeta h)}, \tag{10}$$

where the FL transform, denoted by a tilde, is defined by

$$\tilde{f}(\omega) \equiv \int_0^\infty f(t) e^{-i\omega t}\,\mathrm{d}t, \tag{11}$$

and ζ is given by

$$\zeta = \sqrt{\frac{i\rho\omega}{\eta}}, \tag{12}$$

with ρ, h, and λ being the fluid density, the distance between the top and bottom S–L interfaces, and the friction kernel, respectively (see Appendix A 1).

However, Eq. (10) in the FL form is rather complex, and the solution does not give a clear outlook on the physical aspects of S–L friction. Practically, calculating the FC λ_0 directly from Eq. (10) is not trivial. Regarding this point, in our previous study,[43] we proposed to use the convergence value $\Lambda(\infty)$ as one possible method to obtain λ_0 (see Appendix A 2), where $\Lambda(\infty)$ was related to λ_0 as

$$\Lambda(\infty) \equiv \lim_{t\to\infty} \Lambda(t) = \frac{\lambda_0}{\frac{h}{\eta}\lambda_0 + 2} = \frac{\lambda_0}{\frac{h}{b} + 2}. \tag{13}$$

Thus, λ_0 can be evaluated by

$$\lambda_0 = \frac{2\Lambda(\infty)}{1 - \frac{h}{\eta}\Lambda(\infty)}. \tag{14}$$

Equation (14) indicates that the convergence value of the GK integral $\Lambda(t)$ depends on the liquid height h, and this partly gives an answer to the long-standing issue of the plateau problem of the GK integral.[43] From Eq. (13), it is also clear that a semi-infinite system with $h \to \infty$ results in $\Lambda(\infty) \to 0$, and that the final plateau values $\Lambda(\infty)$ and λ_0 are different. So even in that limit the final plateau does not identify with the friction coefficient. In practice, however, for very large slip lengths, the final plateau appears after a very long time, and only the intermediate plateau can be observed in the simulations, whose value is indeed λ_0.[32]

Although Eq. (14) is simple and insightful, using the convergence value $\Lambda(\infty)$ of the long-range time integration of the correlation function in EMD systems is difficult in practice: for small friction coefficients, the time needed to reach the final plateau becomes very large, and so does the statistical error on $\Lambda(\infty)$; for large friction coefficients, the denominator in Eq. (14) becomes close to zero, leading also to large uncertainties on λ_0. In addition, the viscosity η must be additionally provided, typically calculated using another system, and the liquid hydrodynamic height h must also be determined. Regarding the latter point, it was indicated that the hydrodynamic position of the S–L interface (where the Navier BC applies) was approximately one liquid particle diameter outward from the wall surface for the case of a Lennard–Jones liquid on a flat surface,[25,42,43] while determining the interface position for complex surfaces is not trivial.

In this study, we propose a new method to measure the FC by simplifying Eq. (10) and considering the timescales of the friction kernel. At first, we consider the limit $t_{\mathrm{fk}} \to +0$, i.e., a Markovian Navier BC. Then, the FL transform $\tilde{\lambda}$ of Eq. (9) writes

$$\lim_{t_{\mathrm{fk}}\to+0} \tilde{\lambda}(\omega) = \lambda_0. \tag{15}$$

Note that t_{fk} is usually very small, below several picoseconds except in extreme cases, e.g., supercooled water, and it can be estimated from the autocorrelation function of the S–L friction force $C_{F_{\mathrm{w}}}(t)$, whose short-time behavior corresponds well to the friction kernel $\lambda(t)$.[43]

In addition, we consider the limit $h \to \infty$ in Eq. (10). Then, under these two limits, it follows from Eq. (10) that

$$\lim_{t_{\mathrm{fk}}\to+0} \lim_{h\to\infty} \frac{\tilde{C}_{F_{\mathrm{w}}}(\omega)}{Sk_{\mathrm{B}}T} = \frac{\lambda_0\eta\zeta}{\eta\zeta + \lambda_0}. \tag{16}$$

The inverse FL transform of the RHS in Eq. (16) is analytically obtained as

$$\lim_{t_{\mathrm{fk}}\to+0} \lim_{h\to\infty} \frac{C_{F_{\mathrm{w}}}(t)}{Sk_{\mathrm{B}}T} = \frac{\lambda_0}{t_{\mathrm{slip}}} \exp\left(\frac{t}{t_{\mathrm{slip}}}\right) \times \operatorname{erfc}\left(\sqrt{\frac{t}{t_{\mathrm{slip}}}}\right) - \frac{\lambda_0}{\sqrt{\pi t_{\mathrm{slip}} t}}, \tag{17}$$

introducing a second timescale, t_{slip}, given by

$$t_{\mathrm{slip}} = \frac{\rho b^2}{\eta} = \frac{\rho\eta}{\lambda_0^2}, \tag{18}$$

which can be interpreted as the time of diffusion of the momentum in the liquid over the slip length.

Then, the limit of the GK integral $\Lambda_{\mathrm{mid}}(t)$ results in

$$\begin{aligned}\Lambda_{\mathrm{mid}}(t) &\equiv \lim_{t_{\mathrm{fk}}\to+0} \lim_{h\to\infty} \int_0^t \frac{C_{F_{\mathrm{w}}}(t)}{Sk_{\mathrm{B}}T} dt \\ &= \lambda_0 \exp\left(\frac{t}{t_{\mathrm{slip}}}\right) \operatorname{erfc}\left(\sqrt{\frac{t}{t_{\mathrm{slip}}}}\right).\end{aligned} \tag{19}$$

Equation (19) is the key to obtaining the FC from the GK integral $\Lambda(t)$ in this study. Note that Bocquet and Barrat[29] obtained the same expression as Eq. (17) for a semi-infinite system, i.e., $h \to \infty$.

We see the meaning of the solution including a timescale t_{slip} with respect to the limits related to the other two timescales: the Markovian limit with $t_{\mathrm{fk}} \to +0$ and infinite height $h \to \infty$. The first is supposed to be applicable if the timescale of interest is sufficiently longer than the decay timescale of t_{fk}. For the second limit $h \to \infty$, we consider the diffusion timescale of the velocity information generated on one wall to the opposite wall, given by

$$t_{\mathrm{sys}} \equiv \frac{\rho h^2}{\eta}. \tag{20}$$

This has the same form as t_{slip} in Eq. (18), with the slip length b replaced by h, corresponding to a system timescale defined by the finite liquid height h. Note that the solution in Eq. (19) indeed reproduces the plateau feature if the slip length b and the system height h are large enough. Taking into account that Eq. (19) should hold under the condition of

$$t_{\mathrm{fk}} \ll t \ll t_{\mathrm{sys}}, \tag{21}$$

we propose a calculation method of λ_0 as the FC in Eq. (1) by fitting the GK integral with Eq. (19) in the time range t around the t_{slip}

timescale, satisfying Inequality (21). Indeed, this time separation is supposed to be the key to understanding the S–L friction.[44,45] Note that the present method does not limit the functional form of $\lambda(t)$. In addition, as mentioned in the introduction, Nakano and Sasa[34] proposed another analytical expression for the GK integral based on the time separation as in the present study. They used LFH, whereas we used a different framework starting from the Stokes equation for the fluid and the Langevin equation for the wall, as shown in Appendix A 1.[43] The resulting expressions for the GK integral are different (in particular, the expression of Nakano and Sasa[34] is based on an integral), but the two expressions provide almost identical results in practice, as shown in Appendix B.

III. SIMULATION

All the simulations were performed using the LAMMPS package.[46] We considered a generic Lennard–Jones (LJ) liquid confined between parallel walls; see Fig. 1(a), where we used fcc crystal walls composed of eight atomic layers exposing a (001) face to the liquid; the first neighbors in the solid particles denoted by s were bound by a harmonic potential,

$$\Phi_{\mathrm{h}}^{\mathrm{ss}}(r_{ij}) = \frac{k^{\mathrm{ss}}}{2}(r_{ij}^{\mathrm{ss}} - r_{\mathrm{eq}}^{\mathrm{ss}})^2 \tag{22}$$

with r_{ij}^{ss} the interparticle distance between neighboring solid particles i and j, $r_{\mathrm{eq}}^{\mathrm{ss}} = 0.277$ nm, and $k^{\mathrm{ss}} = 46.8$ N/m. Interactions between fluid particles (ff) and between fluid and solid particles (fs) were modeled by a 12-6 LJ pair potential,

$$\Phi_{\mathrm{LJ}}^{\alpha\beta}(r_{ij}^{\alpha\beta}) = 4\varepsilon^{\alpha\beta}\left[\left(\frac{\sigma^{\alpha\beta}}{r_{ij}^{\alpha\beta}}\right)^{12} - \left(\frac{\sigma^{\alpha\beta}}{r_{ij}^{\alpha\beta}}\right)^{6} + c_2^{\alpha\beta}\left(\frac{r_{ij}^{\alpha\beta}}{r_{\mathrm{c}}^{\alpha\beta}}\right)^2 + c_0^{\alpha\beta}\right], \tag{23}$$

where $r_{ij}^{\alpha\beta}$ is the distance between particles i and j, with $\alpha\beta$ being ff or fs. This LJ interaction was truncated at a cutoff distance of $r_{\mathrm{c}}^{\alpha\beta} = 3.5\sigma^{\mathrm{ff}}$, where the potential $\Phi_{\mathrm{LJ}}^{\alpha\beta}(r_{ij}^{\alpha\beta})$ and the interaction force $-\frac{\mathrm{d}\Phi_{\mathrm{LJ}}^{\alpha\beta}(r_{ij}^{\alpha\beta})}{\mathrm{d}r_{ij}^{\alpha\beta}}$ smoothly vanished at $r_{\mathrm{c}}^{\alpha\beta}$ by adding a quadratic function described by constant coefficients $c_2^{\alpha\beta}$ and $c_0^{\alpha\beta}$.[47] We used $\sigma^{\mathrm{ff}} = 0.34$ nm, $\varepsilon^{\mathrm{ff}} = 121$ K $\cdot\, k_{\mathrm{B}}$, $\sigma^{\mathrm{fs}} = 0.345$ nm, and $\varepsilon^{\mathrm{fs}}$ was varied between $0.155\varepsilon^{\mathrm{ff}}$ and $0.464\varepsilon^{\mathrm{ff}}$ to change the wettability. The contact angle is 136° for $\varepsilon^{\mathrm{fs}} = 0.155\varepsilon^{\mathrm{ff}}$, 79° for $\varepsilon^{\mathrm{fs}} = 0.310\varepsilon^{\mathrm{ff}}$, and complete wetting for $\varepsilon^{\mathrm{fs}} = 0.464\varepsilon^{\mathrm{ff}}$.[12,32] The atomic masses of fluid and wall particles were $m_{\mathrm{f}} = 39.95$ u and $m_{\mathrm{s}} = 195.1$ u. We used periodic boundary conditions along the surface's lateral x and y directions with a box size of $L_x = L_y = 6.27$ nm. The numbers of fluid and wall particles were 6400 and 8192, respectively, and the total system height including walls along the surface's normal z direction was about 12 nm. The distance between the walls was determined by a pressure controlled pre-calculation of 20 ns in which an external force equivalent to the target pressure of 4 MPa was applied to the outermost layer of the top wall.

We compared the GK measurements by EMD with a reference NEMD (Couette) measurement of the friction coefficient. For the NEMD system, the outermost layers of the top and bottom walls have constant velocities: $u_{\mathrm{w}}^{\mathrm{top}} = u_{\mathrm{w}}$ and $u_{\mathrm{w}}^{\mathrm{bot}} = -u_{\mathrm{w}}$ with $u_{\mathrm{w}} = 10$ m/s. Note that the present shear rate with this setting is in the linear response regime.[23,42] The temperature of the system was set to 100 K by applying a Langevin thermostat to the second outermost layer of walls in the xyz-direction for the EMD and the yz-direction excluding the shear direction for the NEMD system. We integrated the equation of motion using the velocity-Verlet algorithm with a time step of 5 fs. The simulation time was 200 ns.

IV. RESULTS AND DISCUSSION

To test the present method, we compared five methods to evaluate λ_0, listed in Table I: λ_{mid} as the present one, and four other methods: λ_{max}, λ_{short}, λ_{∞}, and λ_{NEMD}. The former four are obtained from the GK integral $\Lambda(t)$ in EMD, where λ_{mid} and λ_{short}

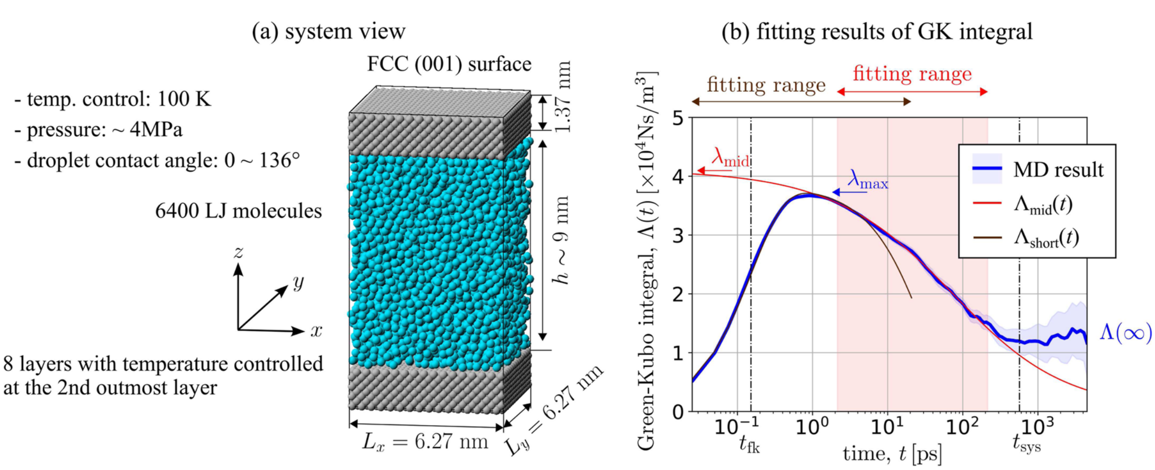

FIG. 1. (a) MD simulation system of LJ liquid between flat fcc walls. (b) (Blue) GK integral $\Lambda(t)$ for $\varepsilon^{\mathrm{fs}} = 0.310\varepsilon^{\mathrm{ff}}$, and fitting curves for (red) $\Lambda_{\mathrm{mid}}(t)$ with Eq. (19) and (brown) $\Lambda_{\mathrm{short}}(t)$ with Eq. (24). The maximum value λ_{max} as well as $\Lambda(\infty)$ used to compute λ_{∞} are also indicated. Finally, the timescales t_{fk} and t_{sys} are represented on the time axis.

TABLE I. Methods to evaluate the friction coefficient λ_0 in Eq. (1) tested in this study.

Symbol	Expression for λ_0 or for $\Lambda(t)$, fitting func.	Timescale[a]	Fit. parameters	System
λ_{mid} (present)	fit. func.: $\Lambda_{\mathrm{mid}}(t) = \lambda_0 \exp\left(\frac{t}{t_{\mathrm{slip}}}\right)\mathrm{erfc}\left(\sqrt{\frac{t}{t_{\mathrm{slip}}}}\right)$[b]	$t \sim t_{\mathrm{slip}}$	λ_0 and t_{slip}	EMD
λ_{short}	fit. func.: $\Lambda_{\mathrm{short}}(t) = \lambda_0(e^{-t/t_1} - e^{-t/t_2})$[c]	$t \sim t_{\mathrm{fk}}$	λ_0, t_1 and t_2	EMD
$\lambda_{\max}$	$\lambda_0 \approx \max[\Lambda(t)]$[d]	$t \sim t_{\mathrm{fk}}$	⋯	EMD
λ_∞	$\lambda_0 \approx \frac{2\Lambda(\infty)}{1-\frac{h}{\eta}\Lambda(\infty)}$[e]	$t > t_{\mathrm{sys}}$	⋯	EMD
λ_{NEMD}	⋯	⋯	⋯	NEMD[f]

[a] t_{fk}, t_{slip}, and t_{sys} are defined in Eqs. (9), (18), and (20), respectively.
[b] Equation (19).
[c] Equation (24).[32]
[d] Equation (6).
[e] Equation (14). Viscosity η and liquid hydrodynamic height h must be additionally calculated.
[f] Shearing the walls with $u_{\mathrm{w}}^{\mathrm{top}} - u_{\mathrm{w}}^{\mathrm{bot}} = 20$ m/s.

are calculated through the fitting of functions to $\Lambda(t)$ for the corresponding timescale ranges, while λ_{NEMD} is evaluated from the NEMD simulation of steady-state Couette-type flows through the direct measurement of τ_{w} and u_{slip} in Eq. (1).[12,21,32,40,48]

Figure 1(b) illustrates the four EMD calculation methods of the FC from the GK integrals $\Lambda(t)$ listed in Table I for a system with $\varepsilon^{\mathrm{fs}} = 0.310\varepsilon^{\mathrm{ff}}$. For λ_{mid}, we fitted the GK integral with Eq. (19) as the red curved-line in Fig. 1(b). The set of fitting parameters is $(\lambda_0, t_{\mathrm{slip}})$, and the fitting range is $(t_{\mathrm{mid}}^{\mathrm{fit}}, 10t_{\mathrm{mid}}^{\mathrm{fit}})$, where 10 values for $t_{\mathrm{mid}}^{\mathrm{fit}}$ were tested in the range of 2.14 and 21.4 ps at equal log-scale intervals. Note that fitting with a monotonically decreasing function for the middle timescale range is similar to the fitting of Nakano and Sasa[34] (see Appendix B). For λ_{short}, we fitted the GK integral $\Lambda(t)$ by

$$\Lambda_{\mathrm{short}}(t) = \lambda_0\left(e^{-\frac{t}{t_1}} - e^{-\frac{t}{t_2}}\right) \tag{24}$$

as proposed in our previous study[32] as the brown line in Fig. 1(b), where the set of fitting parameters is (λ_0, t_1, t_2) and the fitting range is $(0, t_{\mathrm{short}}^{\mathrm{fit}})$ with ten different values of $t_{\mathrm{short}}^{\mathrm{fit}}$ tested in the range of 2.14 and 21.4 ps at equal log-scale intervals. As observed in Fig. 1(b), the red and brown fitting lines corresponding to $\Lambda_{\mathrm{mid}}(t)$ in Eq. (19) and $\Lambda_{\mathrm{short}}(t)$ in Eq. (24) reproduce $\Lambda(t)$ well for their fitting ranges, and from these fitting curves, we extract λ_{mid} (displayed with the red arrow) and λ_{short}. In addition, we calculated the other two FC approximations $\lambda_{\max}$ and λ_∞ from the maximum of $\Lambda(t)$ in Eq. (6) and the convergence value $\Lambda(\infty)$ in Eq. (14). For simple cases, including this example with $\Lambda(t)$ showing a simple behavior of increasing within a short time and decaying after taking the maximum, the former three give similar results, with a slight difference with $\lambda_{\mathrm{mid}}, \lambda_{\mathrm{short}} > \lambda_{\max}$; however, we will see later that it is not the case with structured walls. On the other hand, as mentioned in Sec. I, the final plateau value of $\Lambda(t)$ showed a large fluctuation, as seen in the right-end of the blue curved line in Fig. 1, from which λ_∞ is evaluated, including additional calculations of η and h obtained in different systems.

To determine the liquid height h used to compute λ_∞ and λ_{NEMD}, we considered that the S–L interface position z_{SL} was approximately σ^{fs} outward from the wall surface for the present case.[25,42] While z_{SL} can vary by fractions of a molecular diameter, especially as a function of surface wettability,[25] uncertainties in this interface position do not greatly affect the FC obtained from NEMD, given that the inter-wall distance is sufficiently large and the friction is small, i.e., the slip length is large. However, special care should be taken in cases where friction is large and the slip length becomes comparable to the molecular diameter. With that regard, a strength of the new method we introduce here is that it does not require the hydrodynamic system width as an input, provided the system is sufficiently large.

We defined h as

$$h = z_{\mathrm{SL}}^{\mathrm{top}} - z_{\mathrm{SL}}^{\mathrm{bot}}. \tag{25}$$

The slip velocity u_{slip} used to evaluate λ_{NEMD} was then given by

$$u_{\mathrm{slip}} \equiv \frac{1}{2}\left[\left(u_{\mathrm{w}}^{\mathrm{top}} - u_{\mathrm{w}}^{\mathrm{bot}}\right) - h\left(\frac{\partial u}{\partial z}\right)_{\mathrm{bulk}}\right] = u_{\mathrm{w}} - \frac{h}{2}\left(\frac{\partial u}{\partial z}\right)_{\mathrm{bulk}}, \tag{26}$$

where $\left(\frac{\partial u}{\partial z}\right)_{\mathrm{bulk}}$ was obtained by fitting the average velocity distribution of the liquid bulk with a linear function of z.

Figure 2 shows the FCs obtained for various wettabilities controlled through $\varepsilon^{\mathrm{fs}}$, where we calculated λ_{mid} and λ_{short} as the average for various fitting ranges. The error bars show the uncertainties due to the fitting range and due to the fluctuation of the GK integral $\Lambda(t)$, which gives a larger uncertainty as t increases (the former was much smaller than the latter). Regarding the comparison with the reference NEMD value λ_{NEMD}, λ_{mid}—proposed in this study—reproduced λ_{NEMD} the best in comparison with $\lambda_{\max}$ and λ_{short}, which overall underestimated λ_0, especially for larger FC on more wet surfaces. One can also note that the error bars for λ_∞ were

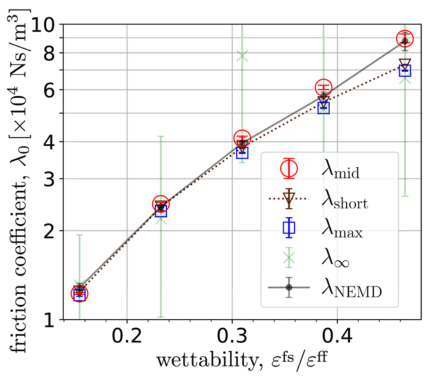

FIG. 2. FC for various wettability ε^{fs}. The calculation methods for each of the five estimates of the FC are shown in Table I.

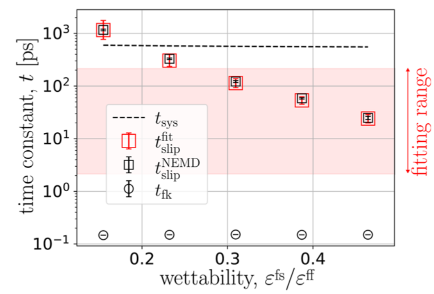

FIG. 3. Time scales as a function of wettability; $t_{sys} = \rho h^2/\eta$, t_{slip}^{fit} obtained as a fitting parameter of Eq. (19), $t_{slip}^{NEMD} = \rho\eta/\lambda_{NEMD}^2$, and t_λ obtained by fitting $\langle F_w(t)F_w(0)\rangle/Sk_BT$ with the Maxwell-type friction in Eq. (9).

too large to precisely evaluate λ_0, at least with the present calculation cost.

As mentioned in Sec. II, there are three key timescales t_{fk}, t_{sys}, and t_{slip} for the GK integral $\Lambda(t)$, and for the present fitting by Eq. (19), the timescale t_{slip} must be separated from t_{fk} and t_{sys}. We estimated the three timescales in the present systems to check this separation. For t_{fk}, considering that the friction kernel $\lambda(t)$ can be well approximated by the correlation function in the RHS of Eq. (27) on a short timescale as[43]

$$\lambda(t) \approx \frac{1}{Sk_B T}\langle F_w(t)F_w(0)\rangle, \tag{27}$$

we fitted the RHS of Eq. (27) with the Maxwell-type friction kernel in Eq. (9). We estimated t_{slip} following two approaches, which we denote by t_{slip}^{mid} and t_{slip}^{NEMD}, respectively: (1) evaluating it as a fitting parameter for λ_{mid} with Eq. (19); and (2) calculating t_{slip} from the FC λ_{NEMD} obtained by NEMD as

$$t_{slip}^{NEMD} \equiv \frac{\rho\eta}{\lambda_{NEMD}^2}. \tag{28}$$

The density and viscosity values ρ and η in Eq. (28) were obtained in the NEMD systems, where η was evaluated by

$$\eta \equiv \frac{\tau_w^{NEMD}}{\left(\frac{\partial u}{\partial z}\right)_{bulk}}, \tag{29}$$

using the average solid–liquid shear force per area τ_w^{NEMD} measured on the solid surface. These values were also used for the evaluation of t_{sys} given by Eq. (20). Since the present systems were under pressure and temperature control, the resulting ρ and η were constant. On the other hand, h slightly depended on the wettability ε^{fs} under this condition with a constant number of fluid particles; hence, t_{sys} slightly depended on the wettability, too.

Figure 3 shows the comparison among the three timescales. For the present system, t_{slip} depended largely on the wettability ε^{fs}, as easily imagined from Eq. (18), with the results of λ_{mid} in Fig. 2. This was in contrast to t_{fk}, which was overall below one picosecond and was almost independent of the wettability. In addition, the system timescale t_{sys} was about several hundreds of picoseconds. Hence, the timescale separation in Inequality (21) was well satisfied for $\varepsilon^{fs} \geq 0.3\varepsilon^{ff}$; however, even for the case of $\varepsilon^{fs} = 0.1\varepsilon^{ff}$ where t_{slip} was larger than t_{sys}, the present result λ_{mid} still gave a good estimate of λ_{NEMD}. This is probably because of the features of the hyperbolic functions sinh and cosh in Eq. (10), which quickly approach the limit for $h \to \infty$ in Eq. (16).

In addition to the analysis on flat surfaces shown above, we applied the FC measurement methods to the S–L friction on grooved surfaces, as exemplified in Fig. 4(a). For each ε^{fs}, two NEMD simulations with shearing in the x- and y-directions were carried out to obtain λ_{NEMD} considering the anisotropic structure of the surface. In the following, we will denote u and v as the velocity along the x- and y-directions, respectively. Since the density and momentum are inhomogeneous in the xy-plane near the wall surface, there is no clear definition of the slip velocity or the interface position. Here, we defined the slip velocity, u_{slip}, or v_{slip}, for the NEMD based on Eqs. (25) and (26) as follows: First, the distributions of mass and momentum density in the x- or y-direction were calculated as the average over the xy-plane. Second, the velocity distribution obtained as momentum density per mass density was fitted only in the bulk part with a linear function to obtain $\left(\frac{\partial u}{\partial z}\right)_{bulk}$ in Eq. (26) or $\left(\frac{\partial v}{\partial z}\right)_{bulk}$ as in the flat wall systems, and finally the slip velocity was obtained by extrapolating the fitted velocity distribution to the positions z_{SL}^{top} and z_{SL}^{bot} in Eq. (25) at σ_{fs} from the top of the grooved wall surface toward the liquid bulk. An EMD simulation was also run for each ε^{fs} to obtain $\Lambda^x(t)$ and $\Lambda^y(t)$ in the two directions using F_w^x and F_w^y as the S–L friction force F_w in Eq. (5).

Figure 4(b) shows an example of the GK integrals $\Lambda^x(t)$ and $\Lambda^y(t)$ for the grooved surface system, with $\varepsilon^{fs} = 0.155\varepsilon^{ff}$. The GK integrals $\Lambda^x(t)$ in the left panel have a complex shape, with a sharp peak in the short timescale below a few picoseconds and a slow decay afterward, which was not observed for $\Lambda^y(t)$ in the right panel nor $\Lambda(t)$ for the flat wall system in Fig. 1(b). This short-time behavior is due to the local vibration of the fluid particles confined in the grooves and is not related to the hydrodynamic motion. We fitted $\Lambda_{short}(t)$ and $\Lambda_{mid}(t)$ to $\Lambda^x(t)$ and $\Lambda^y(t)$ shown with brown and red lines to obtain λ_{short} and λ_{mid} in both directions as well as λ_{max} summarized in Table I. Figure 4(c) shows the comparison between the estimated λ_0 in the x- and y-directions. As imagined from

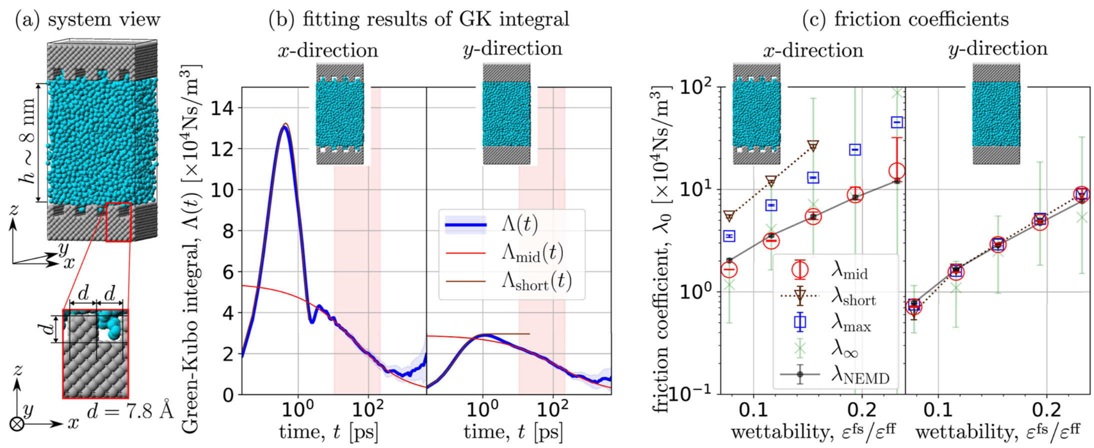

FIG. 4. (a) System view with grooved walls for $\varepsilon^{\mathrm{fs}} = 0.155\varepsilon^{\mathrm{ff}}$. (b) GK integrals $\Lambda(t)$ in the (left) *x*- and (right) *y*-directions and their fitting curves; Blue: GK integral, red: fitting curve for λ_{mid}, and brown: fitting curve for λ_{short}. (c) Obtained FCs for various wettability $\varepsilon^{\mathrm{fs}}$ in the (left) *x*- and (right) *y*-directions; the calculation methods are summarized in Table I.

the complex GK-integrals $\Lambda^x(t)$, λ_{short}, and λ_{max} in the *x*-direction (left panel), using the short timescale resulted in a much larger estimate than λ_{mid}, while the latter corresponded well with the NEMD estimate λ_{NEMD}. On the other hand, for the FC in the *y*-direction (left panel), all EMD estimates except λ_∞ reproduced λ_{NEMD} well. This also indicates that the present NEMD estimate using the above-mentioned definition of the slip velocity was reasonable. Considering the two results, the present FC measurement method λ_{mid} properly evaluates the FC even in this heterogeneous-wall system.

V. CONCLUDING REMARKS

In this study, we proposed a method to calculate the solid–liquid FC from EMD simulations of a liquid confined between parallel solid walls by fitting the GK integral for the timescale range where the GK integral slowly decays with time. The fitting function was derived from an analytical solution of the hydrodynamics equations, considering that the timescales of the friction kernel and bulk viscous dissipation can be separated. We compared the resulting FCs with those obtained with other GK-based methods and with NEMD simulations for a Lennard–Jones liquid confined between flat crystalline walls as well as between grooved walls with different wettability. We showed that the present method extracts the FC with excellent accuracy for various systems, with easy implementation and low calculation costs. We also highlighted two advantages of the method: it makes no assumptions about the time dependence of the friction kernel and does not require the hydrodynamic system width as an input.

ACKNOWLEDGMENTS

H.O., T.O., and Y.Y. were supported by JSPS KAKENHI (Grant Nos. JP21J20580, JP18K03929, JP22H01400 and JP23H01346), Japan, respectively. Y.Y. was also supported by JST CREST (Grant No. JPMJCR18I1), Japan.

AUTHOR DECLARATIONS

Conflict of Interest

The authors have no conflicts to disclose.

Author Contributions

Haruki Oga: Conceptualization (lead); Data curation (lead); Formal analysis (lead); Funding acquisition (equal); Investigation (lead); Methodology (lead); Project administration (supporting); Resources (supporting); Validation (lead); Visualization (lead); Writing – original draft (lead); Writing – review & editing (equal). **Takeshi Omori**: Conceptualization (supporting); Funding acquisition (equal); Investigation (supporting); Methodology (equal); Project administration (supporting); Supervision (supporting); Validation (equal); Writing – original draft (supporting); Writing – review & editing (equal). **Laurent Joly**: Conceptualization (supporting); Investigation (supporting); Methodology (supporting); Project administration (equal); Supervision (supporting); Validation (supporting); Writing – original draft (supporting); Writing – review & editing (equal). **Yasutaka Yamaguchi**: Conceptualization (equal); Data curation (supporting); Formal analysis (supporting); Funding acquisition (lead); Investigation (supporting); Methodology (supporting); Project administration (lead); Resources (lead); Supervision (lead); Validation (supporting); Visualization (equal); Writing – original draft (equal); Writing – review & editing (equal).

DATA AVAILABILITY

The data that support the findings of this study are available from the corresponding author upon reasonable request.

APPENDIX A: DERIVATION OF A THEORETICAL SOLUTION OF THE GK INTEGRAL

1. Derivation through the combination of Langevin equation and Stokes equation

We consider a system where a liquid is confined between two solid walls under no external field and where the top wall is fixed. Let the bottom wall move freely in a wall-tangential direction x; its motion can be described by a generalized Langevin equation,[29]

$$M\frac{\mathrm{d}U}{\mathrm{d}t} = -S\int_0^t \xi(t-t')U(t')\,\mathrm{d}t' + F_{\mathrm{w}}(t), \tag{A1}$$

where M, S, and U are the mass, the surface area, and the x-direction velocity of the bottom wall, respectively; ξ is the friction kernel; and F_{w} is the random force that originates from the direct interaction between the solid and liquid particles. Assuming energy equipartition, Eq. (A1) leads to the fluctuation–dissipation theorem,

$$C_{F_{\mathrm{w}}}(t) \equiv \langle F_{\mathrm{w}}(t)F_{\mathrm{w}}(0)\rangle = Sk_{\mathrm{B}}T\xi(t). \tag{A2}$$

The motion of the liquid in response to the bottom wall motion can be described by the Stokes equation,

$$\frac{\partial u(z,t)}{\partial t} = \frac{\eta}{\rho}\frac{\partial^2 u(z,t)}{\partial z^2} \tag{A3}$$

with the Navier boundary condition defined on the top and bottom hydrodynamic boundaries at $z = 0$ and h, respectively, given by

$$\begin{cases} \eta \left.\dfrac{\partial u(z,t)}{\partial z}\right|_{z=h} = \displaystyle\int_0^t \lambda(t-t')\left[-u(h,t')\right]\mathrm{d}t', \\ \eta \left.\dfrac{\partial u(z,t)}{\partial z}\right|_{z=0} = \displaystyle\int_0^t \lambda(t-t')\left[u(0,t')-U(t')\right]\mathrm{d}t', \end{cases} \tag{A4}$$

where u, t, ρ, η, and λ denote the liquid velocity in the x-direction, the time, the bulk liquid density, the bulk liquid viscosity, and the Navier friction coefficient (FC), respectively. Note that the non-Markovian nature is included in λ.[42] Denoting the Fourier-Laplace transformed variables with a tilde as

$$\tilde{f}(\omega) \equiv \int_0^\infty f(t)e^{-i\omega t}\,\mathrm{d}t, \tag{11}$$

the solution of Eqs. (A3) and (A4) is written in a compact form as $\tilde{u} = \tilde{\gamma}\tilde{U}$ for the liquid velocity on the bottom wall with

$$\tilde{\gamma} = \frac{\tilde{\lambda}\left[\tilde{\lambda}\sinh(\zeta h) + \eta\zeta\cosh(\zeta h)\right]}{(\tilde{\lambda}^2 + \eta^2\zeta^2)\sinh(\zeta h) + 2\tilde{\lambda}\eta\zeta\cosh(\zeta h)}. \tag{A5}$$

Because the first term on the right hand side of Eq. (A1) can also be rewritten as

$$-S\int_0^t \xi(t-t')U(t')\,\mathrm{d}t' = -S\int_0^t \lambda(t-t')\left[U(t') - u(0,t')\right]\mathrm{d}t' \tag{A6}$$

in terms of the slip velocity on the wall, the friction kernel ξ can be written as

$$\tilde{\xi} = \tilde{\lambda}(1-\tilde{\gamma}). \tag{A7}$$

Combined with Eq. (A2), the expression for the force autocorrelation function writes

$$\frac{\tilde{C}_{F_{\mathrm{w}}}}{Sk_BT} = \frac{\tilde{\lambda}\eta\zeta\left[\eta\zeta\sinh(\zeta h) + \tilde{\lambda}\cosh(\zeta h)\right]}{(\tilde{\lambda}^2 + \eta^2\zeta^2)\sinh(\zeta h) + 2\tilde{\lambda}\eta\zeta\cosh(\zeta h)}, \tag{10}$$

where ζ is given by

$$\zeta = \sqrt{\frac{i\rho\omega}{\eta}} \tag{12}$$

as a function of the angular frequency ω.

2. Asymptotic behavior

As one of the possible methods to obtain λ_0, we proposed to use the convergence value $\Lambda(\infty)$ in our previous study,[43] in which we used the following relations:

$$\lim_{\omega\to 0}\frac{\tilde{C}_{F_{\mathrm{w}}}(\omega)}{Sk_BT} = \lim_{\omega\to 0}\int_0^\infty \frac{C_{F_{\mathrm{w}}}(t)}{Sk_BT}e^{-i\omega t}dt = \lim_{t\to\infty}\Lambda(t), \tag{A8}$$

and

$$\lim_{\omega\to 0}\tilde{\lambda}(\omega) = \lim_{\omega\to 0}\int_0^\infty \lambda(t)e^{-i\omega t}dt = \lambda_0. \tag{A9}$$

By inserting Eqs. (10) and (12) into Eq. (A8), it follows for the convergence value of the GK integral that

$$\begin{aligned}\lim_{t\to\infty}\Lambda(t) &= \lim_{\omega\to 0}\frac{\tilde{\lambda}\eta\zeta\left[\eta\zeta\sinh(\zeta h) + \tilde{\lambda}\cosh(\zeta h)\right]}{(\tilde{\lambda}^2 + \eta^2\zeta^2)\sinh(\zeta h) + 2\tilde{\lambda}\eta\zeta\cosh(\zeta h)} \\ &= \lim_{\omega\to 0}\frac{\eta\zeta\tanh(\zeta h) + \tilde{\lambda}}{\left(\frac{\tilde{\lambda}}{\eta\zeta} + \frac{\eta\zeta}{\tilde{\lambda}}\right)\tanh(\zeta h) + 2}.\end{aligned} \tag{A10}$$

By considering Eq. (12) and

$$\lim_{\zeta h\to 0}\frac{\tanh(\zeta h)}{\zeta h} = 1. \tag{A11}$$

Equation (A10) results in

$$\begin{aligned}\lim_{t\to\infty}\Lambda(t) &= \lim_{\omega\to 0}\frac{\eta\zeta\cdot\zeta h\frac{\tanh(\zeta h)}{\zeta h} + \tilde{\lambda}}{\left(\frac{\tilde{\lambda}}{\eta\zeta} + \frac{\eta\zeta}{\tilde{\lambda}}\right)\zeta h\frac{\tanh(\zeta h)}{\zeta h} + 2} \\ &= \frac{\lambda_0}{\frac{h}{\eta}\lambda_0 + 2} = \frac{\lambda_0}{\frac{h}{b} + 2},\end{aligned} \tag{13}$$

where Eq. (4) is used for the final equality. Hence, from Eqs. (4) and (13) λ_0, it can be evaluated by

$$\lambda_0 = \frac{2\Lambda(\infty)}{1 - \frac{h}{\eta}\Lambda(\infty)}. \tag{A12}$$

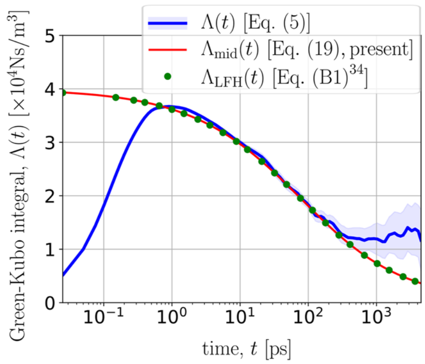

FIG. 5. Comparison of the fitting functions $\Lambda_{\mathrm{LFH}}(t)$ in Eq. (B1) proposed by Nakano and Sasa[34] and in $\Lambda_{\mathrm{mid}}(t)$ in Eq. (19) proposed in the present study for the GK integral $\Lambda(t)$ in Eq. (5).

APPENDIX B: COMPARISON WITH AN APPROXIMATION OF THE GK INTEGRAL BY LFH

Nakano and Sasa[34] proposed, based on the LFH framework, that the GK integral $\Lambda_{\mathrm{LFH}}(t)$ can be approximated by

$$\Lambda_{\mathrm{LFH}}(t) \approx 2\eta \int_0^\infty \frac{\mathrm{d}\omega}{\pi} \frac{q_R(1+q_R b)}{1+2q_R b+2q_R^2 b^2} \frac{\sin \omega t}{\omega} \tag{B1}$$

in Eq. (51) of Ref. 34 for the timescale range $t \ll t_{\mathrm{sys}}$, where q_R is given by

$$q_R = \sqrt{\frac{\omega\rho}{2\eta}}. \tag{B2}$$

Figure 5 shows the comparison of this expression with the present fitting function $\Lambda_{\mathrm{mid}}(t)$ in Eq. (19) for the case of $\varepsilon^{\mathrm{fs}} = 0.310\varepsilon^{\mathrm{ff}}$ (identical to the system in Fig. 1), where $\Lambda_{\mathrm{LFH}}(t)$ was plotted by numerically integrating the RHS of Eq. (B1) using the slip length b obtained in our previous study.[42] The two expressions in Eqs. (B1) and (19) are almost identical in practice, and both fit the original GK integral $\Lambda(t)$ well for $t_{\mathrm{fk}} \ll t \ll t_{\mathrm{sys}}$.

APPENDIX C: VELOCITY DISTRIBUTION OF COUETTE FLOW SYSTEM

Non-equilibrium MD (NEMD) simulations of Couette-type flow were performed to compute the friction coefficient (FC) λ_{NEMD}. Figure 6 shows examples of the distributions of the fluid velocity and density, where two Couette-type MD simulations with shear in the x- and y-directions were carried out for each wettability parameter $\varepsilon^{\mathrm{fs}}$ by moving the top and bottom walls in opposite directions ($\pm x$- or $\pm y$-directions), while a single simulation (x-shear) was run for a flat wall system considering the symmetry of the system. The velocity distributions with shear in the x- and y-directions for the grooved surface systems are shown in blue and pink, respectively, in Fig. 6(b). Indeed, the velocity and density distributions were not completely quasi-one-dimensional, and the streamline was not parallel to the shear direction for the grooved surface system, especially around the wall; e.g., the velocities at two points above the concave and convex regions with the same z-coordinate were different, but the velocity inhomogeneity in the xy-plane quickly vanished, and the time-averaged velocity distribution away from the wall was

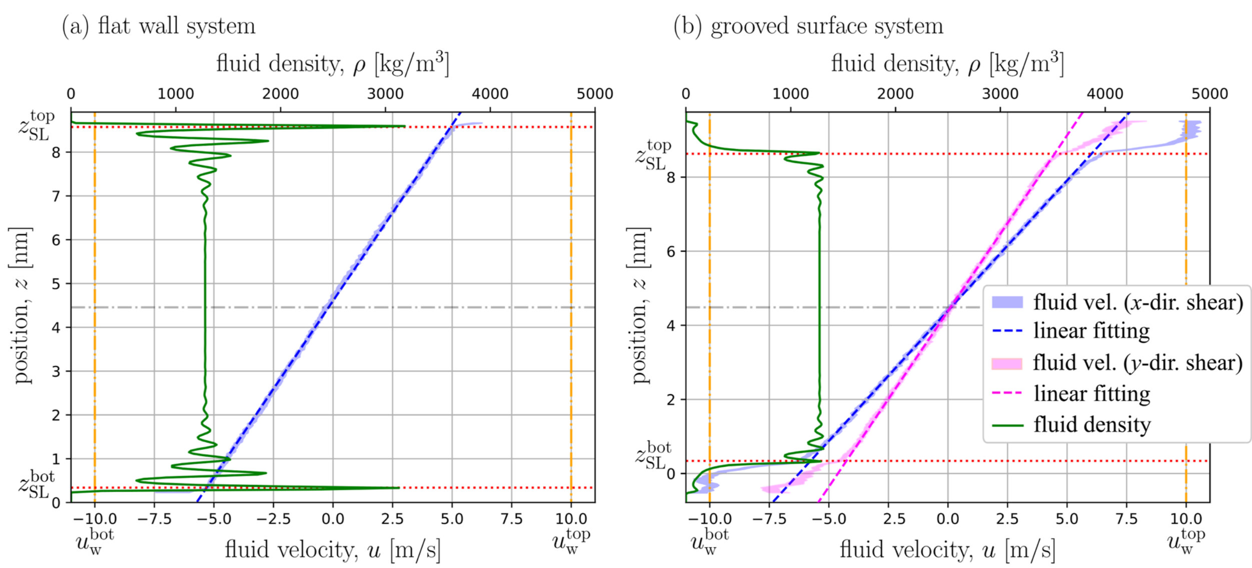

FIG. 6. Distributions of the fluid velocity and density for (a) a flat wall system with $\varepsilon^{\mathrm{fs}} = 0.310\varepsilon^{\mathrm{ff}}$ and (b) a grooved surface system with $\varepsilon^{\mathrm{fs}} = 0.155\varepsilon^{\mathrm{ff}}$. Blue: (solid) fluid velocity distribution for x-direction shear and (dashed) linear fitting. Magenta: (solid) fluid velocity distribution for y-direction shear and (dashed) linear fitting. Green: fluid density. Red dotted lines: positions of the top and bottom solid–liquid interfaces $z_{\mathrm{SL}}^{\mathrm{top}}$ and $z_{\mathrm{SL}}^{\mathrm{bot}}$. Orange dashed lines: wall velocities $u_{\mathrm{w}}^{\mathrm{bot}}$ and $u_{\mathrm{w}}^{\mathrm{top}}$.

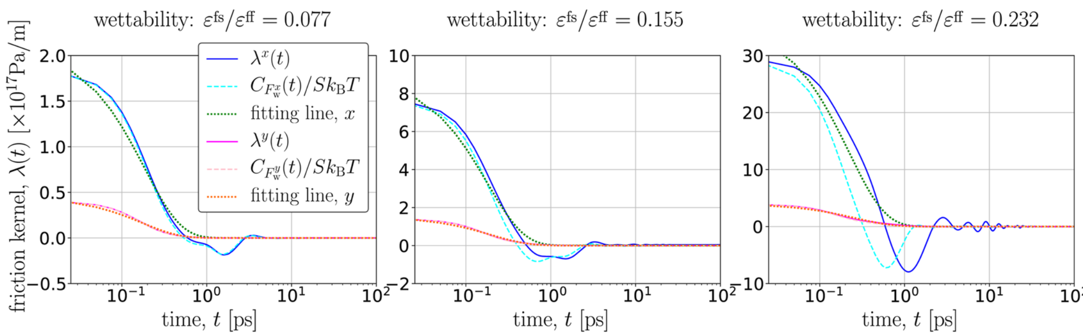

FIG. 7. Friction kernel $\lambda(t)$ for grooved surface systems with wettability parameters $\varepsilon^{\mathrm{fs}}$ of (left) $0.077\varepsilon^{\mathrm{ff}}$, (center) $0.155\varepsilon^{\mathrm{ff}}$, and (right) $0.232\varepsilon^{\mathrm{ff}}$. Blue: (solid) friction kernel $\lambda(t)$ and (dashed) $C_{F_w}(t)/Sk_BT$ for the x-direction. Magenta (solid) friction kernel $\lambda(t)$ and (dashed) $C_{F_w}(t)/Sk_BT$ for the y-direction. The fitting lines with the Maxwell-type kernel in Eq. (9) are shown in green and orange as well.

considered to be quasi-one-dimensional. Considering that the present framework is based on the one-dimensional Stokes equation as described in Appendix A, we averaged the physical quantities in the xy-plane to extract λ_{NEMD} in this study. The positions of the top and bottom solid–liquid interfaces $z_{\mathrm{SL}}^{\mathrm{top}}$ and $z_{\mathrm{SL}}^{\mathrm{bot}}$ are indicated by the red lines in Fig. 6 (see the definition in the main text). In the case of Fig. 6(b), the slip velocity for the shear in the x-direction is smaller than that for the shear in the y-direction.

APPENDIX D: FRICTION KERNEL

To investigate the complex shape of GK integral $\Lambda^x(t)$ in Fig. 4, we numerically solved Eq. (10) with respect to $\lambda(t)$ for the grooved surface system using the method proposed in our previous study;[43] at first, we calculated $\tilde{\lambda}(\omega)$ by numerically solving Eq. (10) by using the FL-transform $\tilde{C}_{F_w}(\omega)$ of the autocorrelation function $C_{F_w}(t)$, and then, we obtained $\lambda(t)$ by performing the inverse-FL transform of $\tilde{\lambda}(\omega)$. Figure 7 shows the results of $\lambda(t)$ obtained for (blue) x- and (magenta) y-directions. The friction kernel $\lambda(t)$ corresponded well with $\frac{C_{F_w}(t)}{Sk_BT}$ shown in cyan and pink in the x- and y-directions, respectively, for small friction coefficients, i.e., for low wettability. This is consistent with the fact that Eq. (27) holds when

$$\sqrt{\frac{\eta t}{\rho}} \ll \min\left(\left|\frac{\eta}{\tilde{\lambda}}\right|, h\right) \tag{D1}$$

is satisfied.[43] We also attempted to fit the kernel by the Maxwell-type kernel in Eq. (9) as shown with green and orange lines. The kernel $\lambda(t)$ can be well approximated by the Maxwell-type kernel for the y-direction, whereas the complex kernel shape cannot be properly expressed by the Maxwell-type kernel for the x-direction. The oscillating behavior of the friction kernel $\lambda(t)$ observed for $\varepsilon^{\mathrm{fs}} = 0.232\varepsilon^{\mathrm{ff}}$ in the x-direction within a short timescale <10 ps is supposed to be due to the vibration of the fluid particles confined in the groove. Indeed, this complex kernel shape $\lambda^x(t)$ is reflected in the complex GK integral $\Lambda^x(t)$ in Fig. 4.

REFERENCES

[1] J. C. Eijkel and A. van den Berg, Microfluid. Nanofluid. **1**, 249 (2005).
[2] W. Sparreboom, A. van den Berg, and J. C. Eijkel, Nat. Nanotechnol. **4**, 713 (2009).
[3] L. Bocquet and E. Charlaix, Chem. Soc. Rev. **39**, 1073 (2010).
[4] R. B. Schoch, J. Han, and P. Renaud, Rev. Mod. Phys. **80**, 839 (2008).
[5] W. Sparreboom, A. van den Berg, and J. C. Eijkel, New J. Phys. **12**, 015004 (2010).
[6] A. Striolo, A. Michaelides, and L. Joly, Annu. Rev. Chem. Biomol. Eng. **7**, 533 (2016).
[7] C. L. M. H. Navier, Mem. Acad. R. Sci. Inst. France **6**, 389 (1823).
[8] K. Falk, F. Sedlmeier, L. Joly, R. R. Netz, and L. Bocquet, Nano Lett. **10**, 4067 (2010).
[9] A. Keerthi, S. Goutham, Y. You, P. Iamprasertkun, R. A. W. Dryfe, A. K. Geim, and B. Radha, Nat. Commun. **12**, 3092 (2021).
[10] K.-T. Chen, Q.-Y. Li, T. Omori, Y. Yamaguchi, T. Ikuta, and K. Takahashi, Carbon **189**, 162 (2021).
[11] D. M. Huang, C. Cottin-Bizonne, C. Ybert, and L. Bocquet, Langmuir **24**, 1442 (2008).
[12] K. Ogawa, H. Oga, H. Kusudo, Y. Yamaguchi, T. Omori, S. Merabia, and L. Joly, Phys. Rev. E **100**, 023101 (2019).
[13] P. A. Thompson and M. O. Robbins, Phys. Rev. A **41**, 6830 (1990).
[14] P. A. Thompson and S. M. Troian, Nature **389**, 360 (1997).
[15] J.-L. Barrat and L. Bocquet, Faraday Discuss. **112**, 119 (1999).
[16] M. Cieplak, J. Koplik, and J. R. Banavar, Phys. Rev. Lett. **86**, 803 (2001).
[17] S. K. Kannam, B. D. Todd, J. S. Hansen, and P. J. Daivis, J. Chem. Phys. **138**, 094701 (2013).
[18] S. K. Bhatia and D. Nicholson, Langmuir **29**, 14519 (2013).
[19] G. Tocci, L. Joly, and A. Michaelides, Nano Lett. **14**, 6872 (2014).
[20] L. Guo, S. Chen, and M. O. Robbins, Eur. Phys. J. Spec. Top. **225**, 1551 (2016).
[21] S. Nakaoka, Y. Yamaguchi, T. Omori, and L. Joly, J. Chem. Phys. **146**, 174702 (2017).
[22] J. P. Ewen, H. Gao, M. H. Müser, and D. Dini, Phys. Chem. Chem. Phys. **21**, 5813 (2019).
[23] S. K. Kannam, B. D. Todd, J. S. Hansen, and P. J. Daivis, J. Chem. Phys. **135**, 144701 (2011).
[24] S. Kumar Kannam, B. D. Todd, J. S. Hansen, and P. J. Daivis, J. Chem. Phys. **136**, 024705 (2012).
[25] C. Herrero, T. Omori, Y. Yamaguchi, and L. Joly, J. Chem. Phys. **151**, 041103 (2019).
[26] L. Bocquet and J.-L. Barrat, Phys. Rev. E **49**, 3079 (1994).
[27] J. Petravic and P. Harrowell, J. Chem. Phys. **127**, 174706 (2007).
[28] J. S. Hansen, B. D. Todd, and P. J. Daivis, Phys. Rev. E **84**, 016313 (2011).

[29] L. Bocquet and J.-L. Barrat, J. Chem. Phys. **139**, 044704 (2013).
[30] K. Huang and I. Szlufarska, Phys. Rev. E **89**, 032119 (2014).
[31] A. Sam, R. Hartkamp, S. K. Kannam, and S. P. Sathian, Nanotechnology **29**, 485404 (2018).
[32] H. Oga, Y. Yamaguchi, T. Omori, S. Merabia, and L. Joly, J. Chem. Phys. **151**, 054502 (2019).
[33] S. Varghese, J. S. Hansen, and B. D. Todd, J. Chem. Phys. **154**, 184707 (2021).
[34] H. Nakano and S. Sasa, Phys. Rev. E **101**, 033109 (2020).
[35] V. P. Sokhan and N. Quirke, Phys. Rev. E **78**, 015301(R) (2008).
[36] N. G. Hadjiconstantinou and M. M. Swisher, Phys. Rev. Fluids **7**, 114203 (2022).
[37] D. Evans and G. Morriss, *Statistical Mechanics of Nonequilibrium Liquids*, 2nd ed. (Cambridge University Press, 2008), pp. 71–72.
[38] P. Español, J. A. de la Torre, and D. Duque-Zumajo, Phys. Rev. E **99**, 022126 (2019).
[39] S. Merabia and K. Termentzidis, Phys. Rev. B **86**, 094303 (2012).
[40] S. Nakaoka, Y. Yamaguchi, T. Omori, and L. Joly, Mech. Eng. Lett. **3**, 17 (2017).
[41] J. C. F. Schulz, A. Schlaich, M. Heyden, R. R. Netz, and J. Kappler, Phys. Rev. Fluids **5**, 103301 (2020).
[42] T. Omori, N. Inoue, L. Joly, S. Merabia, and Y. Yamaguchi, Phys. Rev. Fluids **4**, 114201 (2019).
[43] H. Oga, T. Omori, C. Herrero, S. Merabia, L. Joly, and Y. Yamaguchi, Phys. Rev. Res. **3**, L032019 (2021).
[44] H. Nakano and S.-i. Sasa, J. Stat. Phys. **176**, 312 (2019).
[45] H. Nakano and S. Sasa, Phys. Rev. E **99**, 013106 (2019).
[46] A. P. Thompson, H. M. Aktulga, R. Berger, D. S. Bolintineanu, W. M. Brown, P. S. Crozier, P. J. in't Veld, A. Kohlmeyer, S. G. Moore, T. D. Nguyen, R. Shan, M. J. Stevens, J. Tranchida, C. Trott, and S. J. Plimpton, Comput. Phys. Commun. **271**, 108171 (2022).
[47] S. Nishida, D. Surblys, Y. Yamaguchi, K. Kuroda, M. Kagawa, T. Nakajima, and H. Fujimura, J. Chem. Phys. **140**, 074707 (2014).
[48] S. Nakaoka, Y. Yamaguchi, T. Omori, M. Kagawa, T. Nakajima, and H. Fujimura, Phys. Rev. E **92**, 022402 (2015).